http://dx.doi.org/10.17159/2411-9717/2017/v117n4a11

Iron recovery and phosphorus removal from oolitic high-phosphorus haematite using the FASTMELT® process: a comparative study of two reductants

by H. Tang, X. Fu, Y. Qin, and T. Qi

Synopsis

The FASTMELT® process was developed as an alternative to blast furnace ironmaking; in this process, high-quality molten iron is produced using direct reduction followed by high-temperature slag/metal separation. In this study, iron recovery and phosphorus removal from oolitic high-phosphorus haematite using the FASTMELT® process was investigated. The performance of two reducing agents, coal and wood char, was compared. Direct reduction experiments indicated that with optimized reductant addition, the ore-char and ore-coal briquettes attained metallization values of 82% and 78%, respectively, and residual carbon contents of 0.24 and 2.35%, respectively. The slag/metal separation experiments revealed that molten iron containing 0.41% phosphorus and 0.021% silicon (by mass) was produced from optimally reduced ore-char briquettes, and molten iron containing 0.78% phosphorus and 0.91% silicon from optimally reduced ore–coal briquettes. The study indicates that carbonaceous materials with high CO_2 reactivity are suitable for use in the FASTMELT® process for phosphorus removal and iron recovery from oolitic high-phosphorus haematite.

Keywords

High-phosphorus haematite, FASTMELT, reductant, coal, wood char, phosphorus removal.

Introduction

In China, the general depletion of iron-rich mineral reserves has led to many efforts to exploit low-grade and refractory iron-containing resources for ironmaking (Liu *et al.*, 2014). The efficient utilization of the high-phosphorus oolitic haematite resources in central China has received considerable attention. The available resources of this material total approximately 3.0 billion tons. The oolitic units in the ore exhibit an onion-like structure with phosphorus-containing gangue layers of 2–10 μm thickness. The best concentrate produced from these resources contains approximately 50% iron (Fe) and 0.8–1.2% phosphorus (P) (by mass) (Ai, Yu, and Wei, 2009; Song *et al.*, 2013; Wu, Wen, and Cen, 2011). Further removal of phosphorus from these ores using conventional beneficiation methods is not possible.

Various processes have been developed for processing oolitic high-phosphorus haematite resources and similar minerals around the world. These processes can be categorized as biological (Delvasto *et al.*, 2008; Obot and Anyakwo, 2013), hydrometallurgical (Cheng *et al.*, 1999; Fisher-White, Lovel, and Sparrow, 2012; Ionkov *et al.*, 2013; Jin *et al.*, 2006; Yu, Guo, and Tang, 2013), and pyrometallurgical routes (Bai *et al.*, 2012; Sun *et al.*, 2013; Yu *et al.*, 2013b; Zhu *et al.*, 2013). The pyrometallurgical routes are useful for industrial practice with respect to processing costs, scale, and duration. Most pyrometallurgical routes are conducted using coal-based direct reduction followed by magnetic separation. However, because the phosphorus-containing gangue layers in the oolitic units are extremely thin and closely associated with the haematite layers, the reduced ore-carbon composites must be ground to a particle size of less than 10 μm to attain a sufficient degree of phosphorus removal (Li *et al.*, 2011; Elias and Mitsutaka, 2011; Yin *et al.*, 2012), thereby making these processes energy-intensive.

In addition to blast furnace ironmaking, many new high-efficiency and high-productivity ironmaking processes have recently been developed (Manning and Fruehan, 2001). The FASTMELT® process, which was developed by Kobo Steel Ltd. (Japan) and Midrex Technologies Inc. (USA), has been successfully commercialized. It is a solid-state carbon-based reduction technology and is applicable for processing iron ore as well as iron-oxide-containing materials (Mcclelland and Metius, 2003). Moreover, it has been applied for processing complex iron minerals such as vanadium titanomagnetite (Chen and Chu, 2014). The FASTMELT® process comprises two stages: direct reduction in a rotary hearth furnace (RHF) followed by

* *State Key Laboratory of Advanced Metallurgy, University of Science and Technology Beijing, Beijing, China.*

 ISSN 2225-6253. Paper received May 2015; revised paper received Jul. 2016.

melting-separation in an electric ironmaking furnace. Highly metallized and direct reduced iron (DRI) is fed at high temperature directly into a proprietary melter to produce molten iron. By controlling the chemistry of the reduced ore-carbon composite material, FASTMELT® can be tailored to precisely match the desired molten iron chemistry for steelmaking in a basic oxygen furnace (BOF) or electric arc furnace (EAF) (Lu and Wang, 2003). In our previous studies, a method was developed to obtain a low-phosphorus metal by the melting separation of highly gas-reduced high-phosphorus ore fines (Tang *et al.*, 2014a, 2014b) As the reduction conditions of the FASTMELT® process can be adjusted to obtain DRI of a desired quality, this process can be applied for treating oolitic high-phosphorus haematite if the residual carbon in the DRI can be controlled to a low level. The envisaged technical route is illustrated in Figure 1.

In this study, two common carbonaceous materials, coal and wood char, were employed as reductants. Experiments were conducted using the FASTMELT® process for phosphorus removal and iron recovery from oolitic high-phosphorus haematite, and the results obtained for both reductants were compared.

Experimental

Materials

An oolitic high-phosphorus haematite sample was supplied by Wuhan Iron and Steel Company (China). Table I lists its chemical composition, and an X-ray diffraction (XRD) pattern of the sample is shown in Figure 2. The major minerals in the sample were haematite, quartz, dolomite, clinochlore, and apatite. Figure 3 shows the analysis of the ore by scanning electron microscopy–energy-dispersive X-ray spectrometry (SEM-EDS) analysis. The apatite layers (Point 1 in Figure 3b) and haematite layers (Point 2 in Figure 3b) are alternately developed within the ore particles and are closely associated. The chemical compositions of the wood char and coal reductants are listed in Tables II and III, respectively. All the received samples were crushed and ground to 100% passing 80 μm.

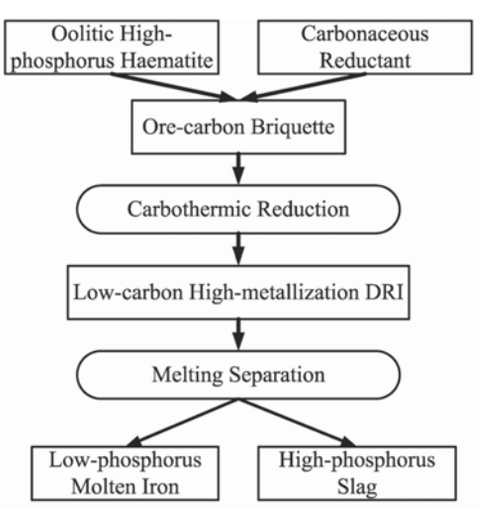

Figure 1—Flow sheet of the envisaged process for treating the oolitic high-phosphorus haematite

Thermal gravimetric analysis

Some coal and wood char fines were carbonized at 1000°C for 3 hours to completely remove the volatiles and moisture, and thermal gravimetric analysis (TGA) was conducted to examine their CO_2 reactivity. A PT-1600 thermal analyzer (LINSEIS, Germany) was employed in these tests. In each run, approximately 20 mg of the devolatilized coal or char sample was used. Each run lasted for 1 hour at 1000°C in a $CO–CO_2$ atmosphere at a gas flow rate of 50 mℓ/min. In the $CO-CO_2$ atmosphere, P_{CO}/P_{CO_2} is 1.0, where P_{CO} and P_{CO_2} are respectively the partial pressures of CO and CO_2. The mass loss of the sample was converted to carbon conversion using the relationship $\Delta m_t / m_c$, where Δm_t is the mass loss at time t and m_c is the total fixed carbon mass in the measured sample, which was calculated on the basis of the data in Tables II and III.

Direct reduction tests

The ore fines were thoroughly mixed with char or coal fines at different carbon mixing ratios (C/O) with the addition of 10% distilled water, 2% organic binder, and 15% CaO powder. C/O is defined as N_C / N_O, where N_C represents the number of moles of fixed carbon in the coal/char fines and N_O is the number of moles of removable oxygen in the ore fines. The organic binder was waste paper pulp, the main component of which is cellulose. The briquettes (6 g, diameter 20 mm, height 10 mm) were formed by pressing the moistened fines under a pressure of 30 MPa using a die. The briquettes were then air-dried for 20 hours, followed by drying in an electric oven at 200°C for 2 hours.

Direct reduction tests were performed in a horizontal alumina tube 850 mm in length and 40 mm in diameter

Table I

Composition of oolitic high-phosphorus iron ore (mass%)

Total Fe	SiO_2	CaO	Al_2O_3	MgO	FeO	MnO_2	P
50.15	12.32	2.68	6.84	0.56	1.56	0.06	1.01

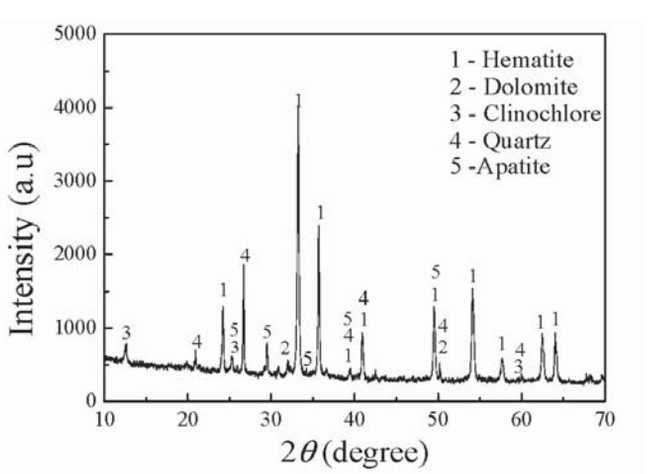

Figure 2—XRD pattern of the high-phosphorus oolitic haematite sample

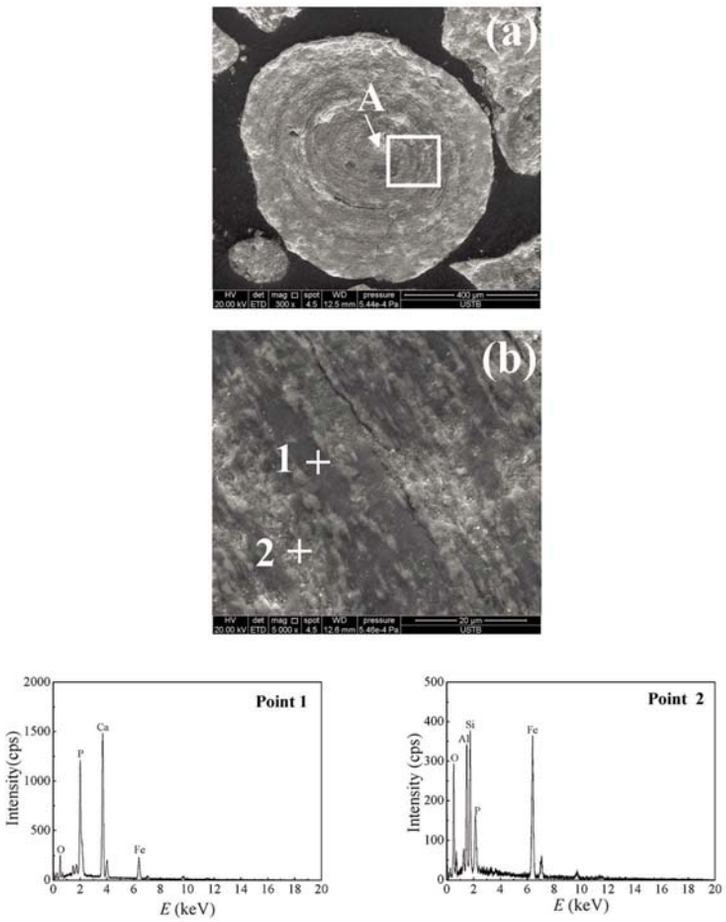

Figure 3—SEM-EDS results of the oolitic high-phosphorus haematite sample. (a) Cross-sectional morphology of the ore particle, (b) microstructure of zone A

Table II

Proximate and ash analysis of the coal sample (mass%)

Proximate analysis (as received)						Ash analysis				
Moisture	Volatile	FC	Ash	S	P	SiO_2	Al_2O_3	Fe_2O_3	CaO	MgO
3.10	6.4	81.4	11.1	0.34	0.026	44.95	32.04	12.66	4.51	0.84

FC: fixed carbon

Table III

Proximate analysis of wood char fines (as received, mass%)

Moisture	Volatile	FC	Ash
3.06	33.51	60.16	2.09

installed inside an electric furnace. The temperature was maintained constant in the reaction zone within ±2°C for a length of 80 mm. The reaction tube was heated from room temperature under a highly pure nitrogen stream. When the temperature of the reaction zone reached the desired value, it was held stable for 30 minutes. In each run, the reaction tube was opened to load two briquettes into the reaction zone and then closed. The reduction began isothermally after nitrogen was replaced with the CO–CO_2 mixture (P_{CO}/P_{CO_2} = 1.0; flow rate = 200 mℓ/min). When the predetermined time was reached, the briquettes were removed from the reaction zone and quenched using a nitrogen stream. After reduction, the reduced briquettes were subjected to metallization and residual carbon (C_R) measurements. Some selected samples were subjected to SEM, EDS, and XRD examination. The SEM and EDS analyses were performed using a Quanta-250 scanning electron microscope (FEI Co., USA). The XRD analysis was performed using an M21X X-ray diffractometer (MAC Science, Japan), and the carbon content analysis was conducted using a CS-2800 infrared carbon sulphur analyser (NCS Co., China). A titrimetric method (iron chloride method) was adopted for measurement of the total iron content (T_{Fe}) and metallic iron content (M_{Fe}). The metallization (M) was calculated using the equation M_{Fe} / T_{Fe} x 100%.

Melting-separation tests

The melting-separation methods described by Tang *et al.* (2014b) were applied. All the runs were conducted at 1550°C and a quench method was adopted. A Si–Mo high-temperature furnace was heated to 1550°C and highly pure argon at a flow rate of 200 mL/min was then introduced into the furnace chamber. In each run, four metallic briquettes were placed in an Al_2O_3 crucible (height 60 mm; diameter

30 mm), which was protected by a graphite crucible. The sample was then quickly inserted into the chamber and the slag/metal separation test was initiated. The melting time was calculated from when the furnace temperature stabilized at 1550°C. The sample was quenched after a melting time of 10 minutes was reached. Some obtained metal samples were subjected to SEM–EDS examination for metal cleanness. All the obtained metal samples were weighed and the phosphorus and silicon contents determined by inductively coupled plasma-atomic emission spectrometry (ICP-AES) using an OPTIMA 7000DV instrument (PE Co., USA). The chemical compositions of the obtained slag samples were examined by energy-dispersive X-ray fluorescence spectrometry (XRF) using an XRF 1800 spectrometer (Shimadzu Co., Japan) with a Rh target X-ray tube, which was operated at 50 kV and 40 mA. Before XRF analysis, the samples were ground to a particle size <10 μm and pressed into briquettes. The XRF data were analysed using an internal fundamental parameter-based quantification method and the analysis was performed by the service provider. The error of the XRF method was within 0.5%. The iron recovery rate (η) was calculated using the equation m_{metal} / m_{iron} x 100%, where m_{metal} is the mass of the obtained metal and m_{iron} the mass of iron in the metallic briquette.

Results and discussion

CO_2 reactivity of reductant

The CO_2 gasification reaction of a carbonaceous reductant is described by Equation [1]

$$C+CO_2 = 2CO. \quad [1]$$

To simulate the coal/char gasification behaviour during the direct reduction of the briquette, a temperature of 1000°C and an atmosphere of P_{CO}/P_{CO_2} = 1 were adopted. The TGA results are presented in Figure 4. The CO_2 reactivity of the wood char was found to be significantly superior to that of the coal. The wood char fines were completely gasified within 10 minutes at 1000°C, but the coal fines only reached a gasification efficiency of approximately 0.4 after 1 hour.

Optimization of reduction conditions

To obtain metallized briquettes with low residual carbon and high metallization, the reduction conditions for each briquette needed to be optimized. Based on the RHF conventional operation conditions and the target of the present research, an atmosphere of P_{CO}/P_{CO_2} = 1 was adopted, C/O was set to be not greater than 1.0, and the temperature range was from 1000°C to 1200°C. Under these conditions, the reduction behaviours of the ore-char and ore-coal briquettes were investigated and their respective reduction conditions were optimized.

The results of the reduction experiments for the ore-char briquette are shown in Figure 5. The briquette exhibited a maximum metallization at 10–15 minutes in the course of reduction for all cases. Figure 5a shows the effect of temperature on the briquette reduction. The maximum metallization of the briquette was low (75%) at 1000°C and reached 84% at 1100°C; however, no substantial improvement was observed at 1200°C. Figure 5b shows the effect of C/O on the briquette reduction. The maximum metallization of the briquette was 79% for a C/O of 0.7 and increased to 84% for a C/O of 0.8; however, little improvement was observed upon further increasing the C/O to 0.9. These findings indicate that a C/O of 0.8 and temperature of 1100°C are sufficient to achieve a high metallization for the ore-char briquette.

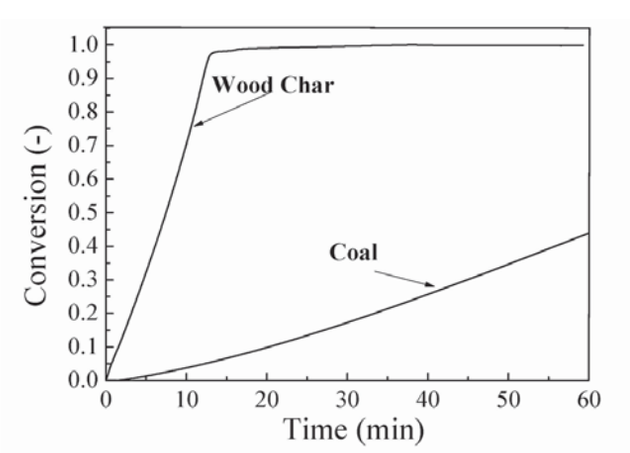

Figure 4—Gasification behaviour of coal and wood char

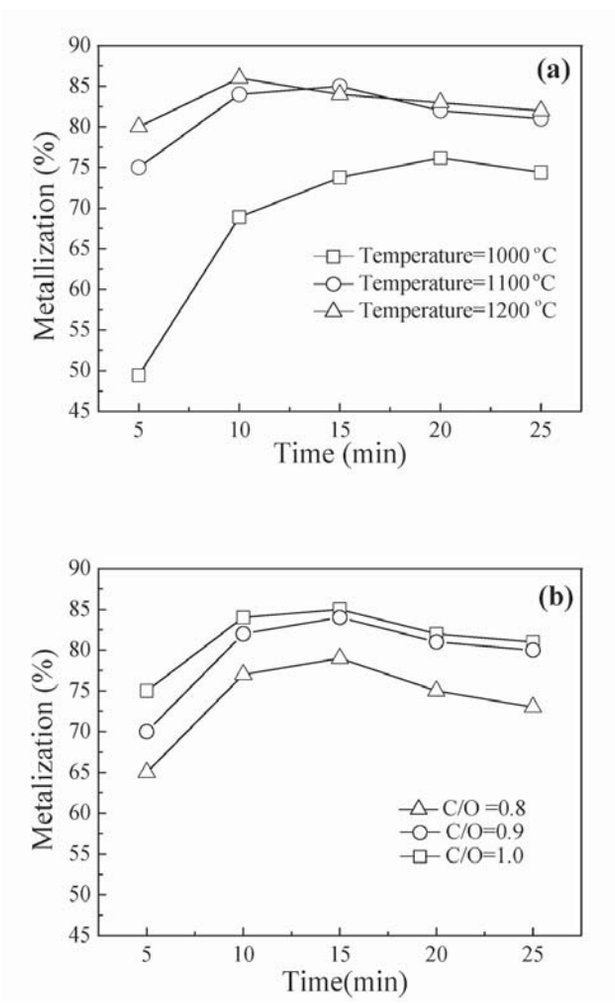

Figure 5 – Reduction behaviour of the ore-char briquette (experimental error <3%). (a) Effect of temperature (C/O=0.9), (b) effect of C/O (temperature=1100°C)

The results of the reduction experiments for the ore-coal briquette are shown in Figure 6. Figure 6a shows that the reduction rate increases with increasing temperature. At 1200°C, a maximum metallization of 82% was attained for the ore-coal briquette at 15 minutes. The metallization increased with increasing time, with final metallization values of 80% and 60% at 1100°C and 1000°C respectively. Figure 6b shows that the reduction rate was enhanced by increasing the C/O value. These findings indicate that for the ore-coal briquette, increases in both temperature and C/O have a positive effect on the briquette reduction. However, a comparison of Figures 6a and 6b indicates that the effect of temperature is more significant than that of C/O. With the aim of controlling the residual carbon to a low level, the preferred temperature, and C/O are considered to be 1200°C and 0.9, respectively.

To minimize the residual carbon content in the reduced briquette, the variation in the residual carbon content with time was examined for each briquette under the identified optimized temperature and C/O conditions. The results are shown in Figure 7. The corresponding metallization variation of each briquette is also plotted. After reducing the ore-char and ore-coal briquettes for 20 minutes, the residual carbon contents decreased to 0.24% (Figure 7a) and 2.35% (Figure 7b), respectively. In both cases, no significant decrease of the residual carbon content was achieved by further increasing the reduction time. Therefore, the optimal reduction time was 20 minutes for both types of briquette.

The above analysis indicates that by optimizing the temperature, C/O, and reduction time, briquettes with a metallization of 82% and residual carbon content of 0.24% can be obtained using ore-char briquettes, and a metallization of 78% and residual carbon content of 2.35% using ore-coal briquettes.

The optimum reduction conditions for the briquette are closely associated with the properties of the reductant employed. In the briquette reduction, in addition to Reaction [1], Reactions [2-4] are involved in the process:

$$Fe_xO_y+C=Fe_xO_{y-1}+CO \quad [2]$$

$$Fe_xO_y+CO=Fe_xO_{y-1}+CO_2 \quad [3]$$

$$Fe+CO_2=FeO+CO \quad [4]$$

The fast reduction of the briquette in the initial stage was attributed to the release of CO-rich and H_2-rich volatiles from the reducing agent and Reaction [2]. A reductant with a higher volatile content was advantageous in this stage; therefore, the ore-char briquette exhibited a higher initial reduction rate than the ore-coal briquette under similar

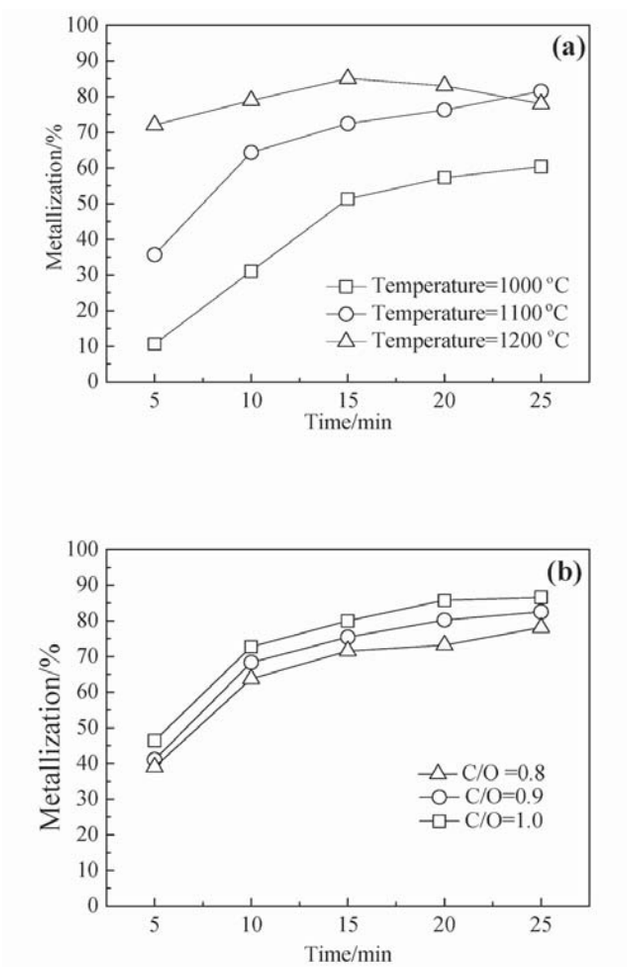

Figure 6 – Reduction behaviour of ore-coal briquette (experimental error <3%. (a) Effect of temperature (C/O=0.9), (b) effect of C/O (temperature=1100°C)

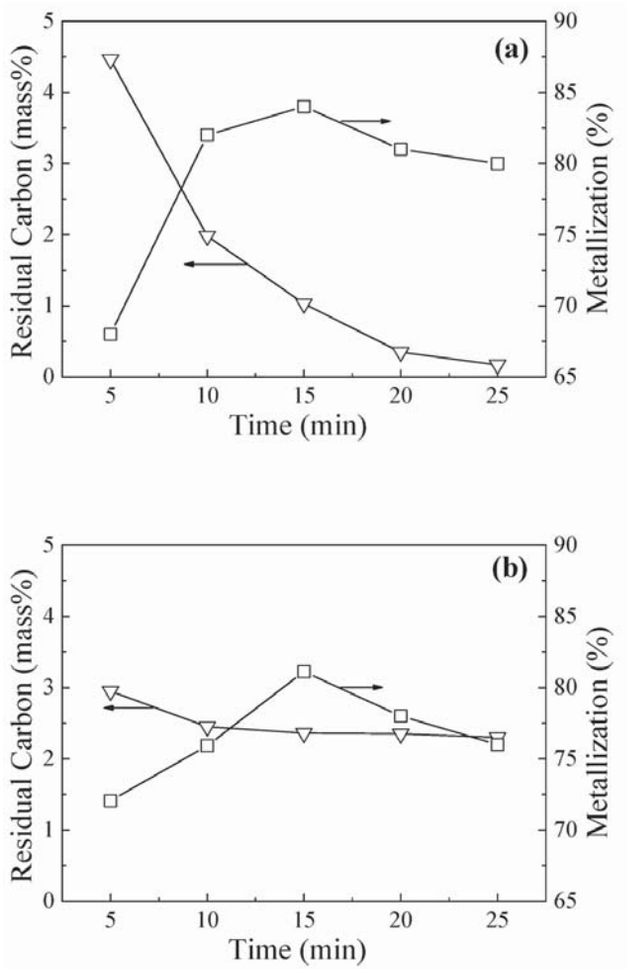

Figure 7—Variation of residual carbon in the briquette with time. (a) Ore-char briquette (temperature=1100°C, C/O=0.8), (b) ore-coal briquette (temperature=1200°C, C/O=0.9)

reduction conditions. With the reduction developing, Reactions [1] and [3] dominated the reduction process. Compared with the briquette containing a reductant with low CO_2 reactivity, the briquette containing a reductant with high CO_2 reactivity exhibited high internal CO pressure, which could be approximately 1.0 atmospheres; thus, the high reduction rate of Reaction [3] could be obtained under a given temperature and given C/O. Therefore, compared with the ore-coal briquette, the ore-char briquette could reach a high metallization above 80% under a low temperature and low C/O. After the briquette reached its maximum metallization, the reduction of the ore fines ceased (the rate of Reaction [3] was zero), and atmospheric CO_2 started to invade the briquette, Reaction [1] continued and Reaction [4] occurred. Figures 4 and 5 show that under the employed atmosphere, re-oxidation was not severe at this stage. Further decrease of the residual carbon content of the briquette still depended on the CO_2 reactivity of the reductant. As the wood char exhibited a much higher CO_2 reactivity than the coal, the decrease of the residual carbon content was obvious in the ore-char briquette (Figure 7a) but negligible in the ore-coal briquette (Figure 7b).

Characteristics of reduced briquettes

XRD patterns of the optimally reduced ore-char and ore-coal briquettes are presented in Figure 8. Figure 8a shows that the major phases in the reduced ore-char briquette were metallic iron, wustite, quartz, and apatite. Figure 8b shows that the major phases in the reduced ore-coal briquette were metallic iron, wustite, and apatite.

The microstructures of the optimally reduced ore-char and ore-coal briquettes are presented in Figure 9 and Figure 10, respectively. Comparison of Figure 9a and Figure 10a with Figure 3(a) indicates that the oolitic units were completely destroyed after the reduction of both briquettes. Comparison of Figure 8a with Figure 9a indicates that the ore-char briquette became more porous after reduction than the ore-coal briquette; furthermore, the coalescence of iron particles in the reduced ore-char briquette was less developed. These phenomena were attributed to the reduction temperature. The metallized ore-coal briquette was obtained at 1200°C and the metallized ore-char briquette at 1100°C. At 1200°C, many complex oxides were formed by gangue components combining with unreduced iron oxide (wustite). Some of these complex oxides or their mixtures (*e.g.,* 2FeO SiO_2, 2FeO SiO_2-SiO_2, and 2FeO SiO_2-FeO) have low melting points and thus formed glassy phases, prompting sintering but also enhancing the coalescence of the iron particles. The EDS results of point 2 in Figure 9b and point 2 in Figure 10b indicate that in both briquettes, calcium phosphate was present in the gangue phase but not in the metallic iron phase. The apatite layers were also observed to be broken into very small particles (less than 10 μm) after reduction.

In the presence of carbon and SiO_2, Reactions [5-6] (Ye and Hu, 2002) are involved in the phosphate phase transition.

$$Ca_3(PO_4)2+3SiO_2+5C=3CaSiO_3+5CO(g)+P_2(g) \quad [5]$$

$$\Delta G^0=1519.19-1.032T \text{ (kJ/mol)}$$

$$6Fe+P_2(g)=2Fe_3P \quad [6]$$

$$\Delta G^0=-630.22+0.18T \text{ (kJ/mol)}.$$

The standard free energy (ΔG^0) of Reaction [5] is 96.97 kJ/mol at 1100°C and –3.424 kJ/mol at 1200°C, which indicates that Reaction [5] may occur at temperatures under 1200°C; therefore, phosphorus can be transferred into the metal phase through Reactions [5] and [6] during the reduction of the ore-coal briquette. However, from Figure 8b and Figure 10b, it could be concluded that the phosphorus transfer had not occurred to any great extent in the course of reduction of the ore-coal briquette because Reaction [5] was kinetically hindered by the glassy phases.

Results of melting-separation

The melting-separation results for the optimally reduced ore-char briquettes (sample A) and ore-coal briquettes (sample B) are listed in Table IV. The chemical compositions of the obtained slag samples are listed in Table V.

Table IV reveals that the iron recoveries from samples A and B were on the same level of approximately 80%. For sample A, the obtained metal contained low Si (0.021%) and low C (0.020%). For sample B, although residual carbon content was high at 2.35%, the obtained metal had a low C (0.017%) but high Si (0.91%) content. In the melting-separation process, gangue particles, metallic iron particles,

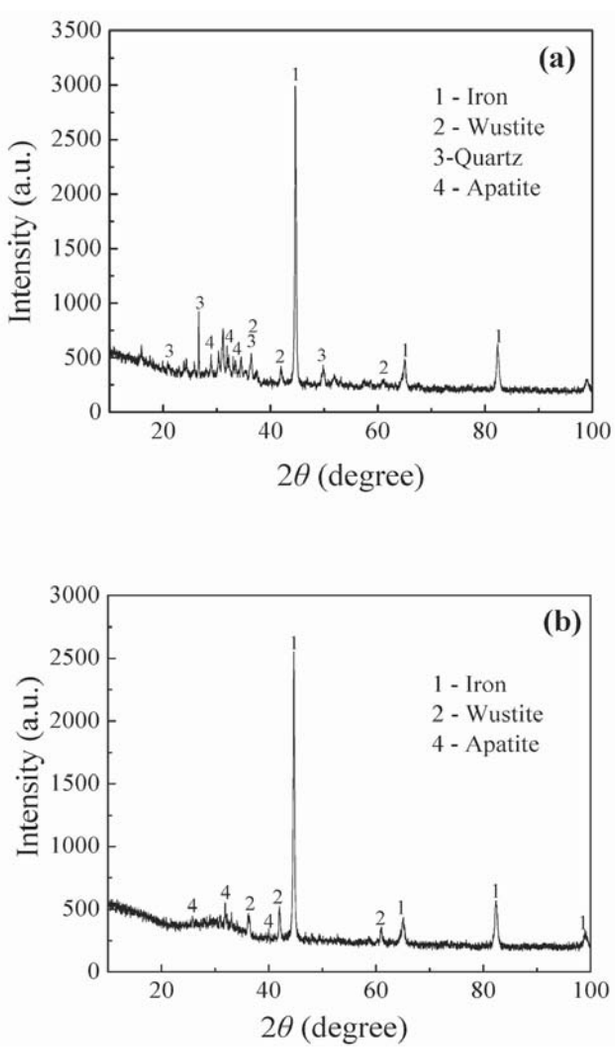

Figure 8—XRD patterns of the optimally reduced briquettes. (a) Ore-char briquette, (b) ore-coal briquette

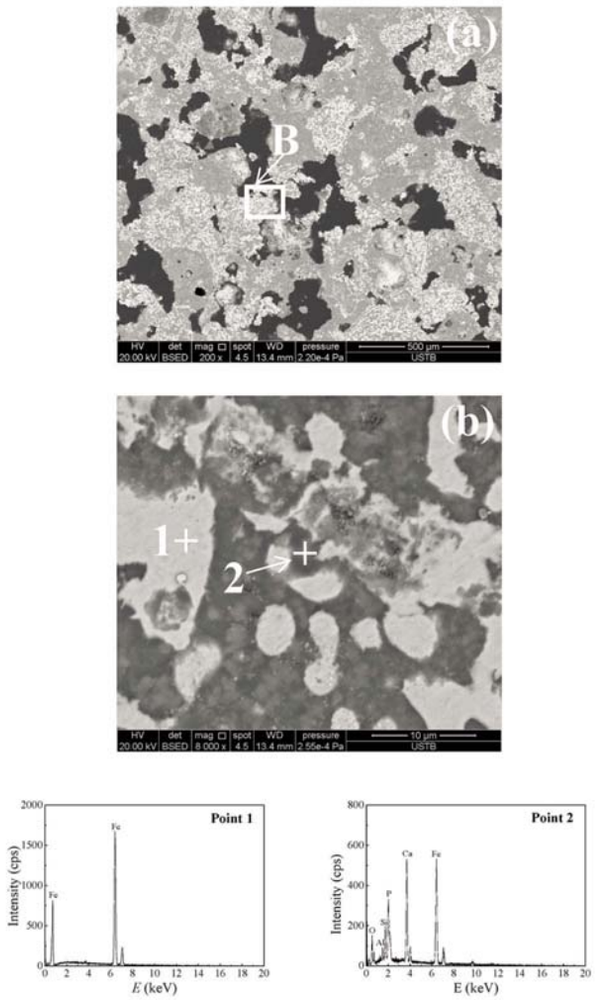

Figure 9—SEM-EDS results for the optimally reduced ore-char briquette. (a) Morphology of cross-section, (b) microstructure of zone B

and residual coal/char particles were in intimate contact in the briquette. Therefore, most of residual coal/char particles inevitably reacted with FeO and SiO_2 through Reactions [7] and [8] and the remaining carbon particles were dissolved in the molten iron.

$$FeO(1)+C=Fe(1)+CO \quad [7]$$

$$SiO_2(1)+2C+2Fe(1)=2SiFe(1)+2CO \quad [8]$$

Compared with sample A, the occurrences of Reactions [7] and [8] in Sample B were apparent as Sample B had a high residual carbon content.

The phosphorus contents of the metals obtained from samples A and B (Table IV) were quite different, at 0.41% and 0.78% respectively.

Because all the obtained metals exhibited very low carbon contents, the phosphorus behaviour in the melting-separation process could be predicted using the ion and molecular coexistence theory (IMCT) (Yang *et al.*, 2011) assuming that the melting system was in or close to thermodynamic equilibrium. For applying IMCT, the slag system was considered to be CaO–FeO–Al_2O_3–P_2O_5–SiO_2 according to Table V, and the structural units and thermodynamic data were determined according to the method of Yang *et al.*, (2011). The phosphorus partition ratio was then calculated using Equation [9]. The activity of phosphorus in molten iron was simply considered to be equal to its mass concentration in the present calculations.

$$L_P=\frac{(\%\ P_2O_5)}{[\%\ P]^2}=141.94N_{FeO}^5(\sum n)K_0(1+K_{3FeO\cdot P_2O_5}N_{FeO}^3+K_{4FeO\cdot P_2O_5}N_{FeO}^4+K_{2CaO\cdot P_2O_5}N_{CaO}^2+K_{3CaO\cdot P_2O_5}N_{CaO}^3+K_{4CaO\cdot P_2O_5}N_{CaO}^4) \quad [9]$$

where $(\%P_2O_5)$ is the mass percentage of P_2O_5 in the slag, [%P] is the mass percentage of phosphorus in the metal, K_i is the chemical equilibrium constant, Σn is the number of moles of total units, and N_i is the mass action concentration represented by the mole fraction.

For sample A, the calculated L_P was 26 and the measured L_P was 18, which indicates that the model prediction result is in relatively good agreement with the experimental result. For sample B, the model-predicted L_P was 22 and the measured L_P was 4, which indicates there is a large deviation between the model prediction and experimental result.

In fact, Reaction [10] occurred in the melting-separation process of sample B because [%Si] in the obtained metal was high.

$$[Si]+2(FeO)=2Fe+(SiO_2) \quad [10]$$

where the round brackets indicate a species in the slag and square brackets indicate a species in the metal phase.

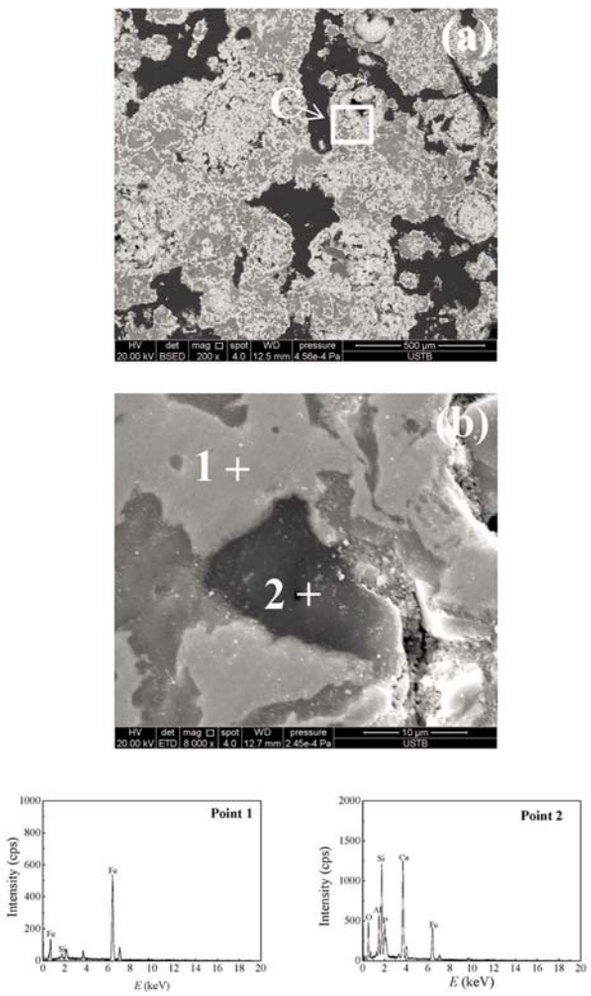

Figure 10 – SEM-EDS results for the optimally reduced ore-coal briquette. (a) Morphology of the cross-section, (b) microstructure of zone C

Table IV

Melting separation results

	Metallized briquette		Molten iron			
	R_C	M	η	P	Si	C
	mass%	%	%	mass%	mass%	mass%
Sample A	0.24	82	78	0.41	0.021	0.020
Sample B	2.35	78	81	0.78	0.91	0.017

Samples A and B are the optimally reduced ore-char briquettes and ore-coal briquettes, respectively

Table V

Compositions of the obtained slags (mass%)

	FeO	SiO_2	Al_2O_3	CaO	P_2O_5	Other
Sample A	19	25	20	30	3.09	2.91
Sample B	15	24	22	32	2.45	4.55

Samples A and B are the optimally reduced ore-char briquettes and ore-coal briquettes, respectively

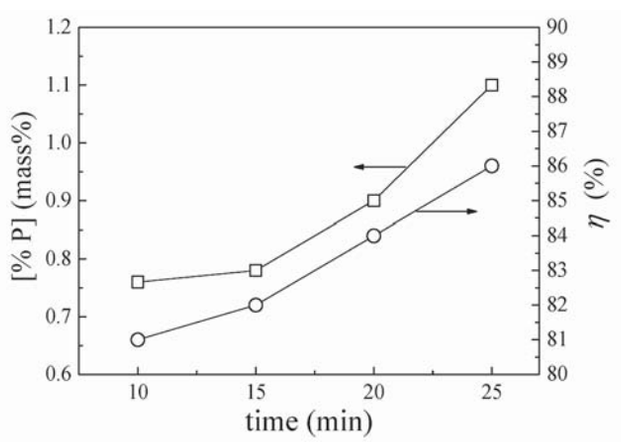

Figure 11—Variation of [%P] and η with smelting time for Sample B

The occurrence of Reaction [10] indicates that the melting system of sample B may not be under equilibrium using the melting method employed in the present research. The variations of [%P] and η with melting time were then investigated for sample B, and the results are presented in Figure 11. Both [%P] and η increased with increasing melting

time. Reaction [10] would result in a decrease in the FeO content and an increase in the SiO_2 content in the slag; therefore, it has a negative effect on L_P as per the IMCT model. Therefore, increasing the melting time is not beneficial for reducing [%P] in the metal obtained from sample B.

Molten iron with a P content less than 0.45% and Si content less than 0.15% can be easily processed currently in BOF or EAF steelmaking (Chen and He, 2014; Zhang *et al.*, 2013). It is thus considered that wood char is a more suitable reductant in the proposed method than the coal used in this study.

Conclusions

The application of the FASTMELT® process for the removal of phosphorus from oolitic high-phosphorus haematite was investigated experimentally using two reducing agents, wood char and coal.

In the direct reduction stage, under their respective optimized conditions, the ore-char and ore-coal briquettes reached metallization degrees of 82% and 78% and residual carbon contents of 0.24% and 2.35% by mass, respectively. Phosphorus remained in the gangue as apatite after reduction of both briquettes.

In the melting-separation stage, from the optimally reduced ore-char briquettes, molten iron with P content of 0.41% and Si content of 0.021% could be obtained; from the reduced ore-coal briquettes, molten iron with P content of 0.78% and Si content of 0.91% could be obtained.

The study indicated that carbonaceous materials with high CO_2 reactivity are preferred for the proposed method.

Acknowledgements

The authors wish to thank the Chinese Natural Science Foundation for support under the Project No. 51144010. Thanks are also given to State Key Laboratory of Advanced Metallurgy USTB for financial support.

References

Ai, G., Yu, X., and Wei, Z. 2009. Research on iron increase and dephosphorization of refractory high phosphorus hematite-limonite ore. *Mining and Metallurgy Engineering*, vol. 29. pp. 43–49 (in Chinese).

Bai, S., Wen, S., Liu, D., Zhang, W., and Cao, Q. 2012. Beneficiation of high phosphorus limonite ore by sodium carbonate-added carbothermic reduction. *ISIJ International*, vol. 52. pp. 1757–1763.

Chen, S.Y. and Chu, M.S. 2014. A new process for the recovery of iron, vanadium, and titanium from vanadium titanomagnetite. *Journal of the Southern African Institute of Mining and Metallurgy*, vol.114. pp. 481–487.

Chen, G. and He, S. 2014. Thermodynamic analysis and experimental study of manganese ore alloy and dephosphorization in converter steelmaking. *Journal of the Southern African Institute of Mining and Metallurgy,* vol.114. pp. 391–399.

Cheng, C.Y., Misra V.N., Clough, J., and Mun, R. 1999. Dephosphorization of western Australian iron ore by hydrometallurgical process. *Minerals Engineering,* vol. 9. pp. 1083–1092.

Delvasto, P., Valverde, A., Ballester, A., Muno, J.A., Gonzalez, F., Blazquez, M.L., Igual, J.M., and Garcia-Balboa C. 2008. Diversity and activity of phosphate bioleaching bacteria from a high-phosphorus iron ore. *Hydrometallurgy*, vol. 92. pp. 124–129.

Elias, M. and Mitsutaka, H. 2011. Dephosphorization treatment of high phosphorus iron ore by pre-reduction, air jet milling and screening methods, *ISIJ International*, vol. 51. pp. 544-551.

Fisher-White, M.J., Lovel, R.R., and Sparrow, G.J. 2012. Phosphorus removal from goethitic iron ore with a low temperature heat treatment and a caustic leach. *ISIJ International*, vol. 53. pp. 797–803.

Ionkov, K., Gaydardzhiev, S., Araujo, A., Bastin, D., and Lacoste, M. 2013. Amenability for processing of oolitic iron ore concentrate for phosphorus removal. *Minerals Engineering*, vol. 46. pp. 119–127.

Jin Y., Jiang, T., Yang, Y., Li, Q., Li, G., and Guo, Y. 2006. Removal of phosphorus from iron ores by chemical leaching. *Journal of Central South University (Technology)*, vol. 13. pp. 673–677.

Li, S., Zhang., Y., Gao, J., Li, J., Chen, P., Liu, R., and Wang, Y. 2011. Experimental study on gas-based reduction of ultra-fine oolitic high-phosphorus hematite powder. *Chinese Journal of Process Engineering,* vol. 20. pp. 599–605 (in Chinese).

Liu, S., Zhao, Y., Wang, W., and Wen S. 2014. Beneficiation of a low grade hematite-magnetite ore in China. *Minerals and Metallurgical Processing*, vol. 31. pp. 136–142.

Lu, W. and Wang, F. 2003. Mechanisms of reduction of iron ore/coal agglomerates and scientific issues in RHF. *Mineral Processing and Extractive Metallurgy Review*, vol. 24. pp. 293–322.

Manning C.P. and Fruehan, R.J. 2001. Emerging technologies for iron and steelmaking. *JOM*, vol. 63. pp. 36–43.

Mcclelland, J.M. and Metius G.E. 2003. Recycling ferrous and nonferrous waste streams with FASTMET. *JOM,* vol. 65. pp. 30-34.

Obot O.W. and Anyakwo, C.N. 2012. Phosphorus removal from Nigeria's Agbaja iron ore by solubilization with *Eurotium herbariorum*. J*ournal of Microbiology and Antimicrobials*, vol. 4. pp. 115–122.

Song, S., Campos-Toro, E.F., Zhang, Y., and Lopez-VAaldivieso, A. 2013. Morphological and mineralogical characterizations of oolitic ore in the Exi region, China, *International Journal of Minerals Metallurgy and Materials*, vol. 20. pp. 113–118.

Sun, Y., Han, Y., Gao, P., Wang, Z., and Ren, D. 2013. Recovery of iron from high phosphorus oolitic iron ore using coal-based reduction followed by magnetic separation, *International Journal of Minerals Metallurgy and Materials*, vol. 20, pp. 411–419.

Tang, H., Liu, W., Zhang, H., and Guo, Z. 2014a. Effect of microwave treatment upon processing oolitic high-phosphorus iron ore for phosphorus removal, *Metallurgical and Materials Transactions B*, vol.45. pp. 1683–1693.

Tang, H., Ma, L., Wang, J., and Guo, Z., 2014b. Slag-metal separation process of gas-reduced high phosphorus iron ore fines, J*ournal of Iron and Steel Research International*, vol. 21. pp. 1009–1015.

Wu, J., Wen, Z., and Cen, M. 2011. Development of technologies for high phosphorus oolitic hematite utilization. *Steel Research International*, vol. 82. pp. 494–500.

Yang, X., Shi, C., Zhang, M., Duan, J., and Zhang, J. 2011. A thermodynamic model of phosphate capacity for $CaO-SiO_2$ -MgO-FeO-Fe_2O_3-MnO-Al_2O_3-P_2O_5 slags equilibrated with molten steel during a top–bottom combined blown converter steelmaking process based on the ion and molecule coexistence theory. *Metallurgical and Materials Transactions B*, vol. 42. pp. 951–977.

Ye, D. and Hu. J. 2002. Thermodynamic Data of Inorganic Substances. 2nd edn. Metallurgy Industry Press, Beijing, China.

Yin, J., Lv, X., Bai, C., Qiu, G., Ma, S., and Xie, B. 2012. Dephosphorization of iron ore bearing high phosphorous by carbothermic reduction assisted with microwave and magnetic separation. *ISIJ International*, vol. 52. pp. 1579–1584.

Yu, J., Guo, Z., and Tang, H. 2013. Dephosphorization treatment of high phosphorus oolitic iron ore by hydrometallurgical process and leaching kinetics. *ISIJ International*, vol. 53. pp. 2056–2064.

Yu, W., Sun, T., Kou, J., Wei, Y., Xu, C., and Liu, Z. 2013. The function of $Ca(OH)_2$ and Na_2CO_3 as additive on the reduction of high-phosphorus oolitic hematite-coal mixed pellets. *ISIJ International*, vol. 53. pp. 427–433.

Zhang, X., Xie, B., Li, H. Y., Diao, J., and Ji, C.Q. 2013. Coupled reaction kinetics of duplex steelmaking process for high phosphorus hot metal. *Ironmaking and Steelmaking*, vol. 40. pp. 282–289.

Zhu, D., Chun, T., Pan, J., Lu, L., and He, Z. 2013. Upgrading and dephosphorization of Western Australian iron ore using reduction roasting by adding sodium carbonate, *International Journal of Minerals Metallurgy and Materials*, vol. 20. pp. 505–513. ◆